Biomedicine & Pharmacotherapy 111 (2019) 602–612

Contents lists available at ScienceDirect

Biomedicine & Pharmacotherapy

journal homepage: www.elsevier.com/locate/biopha

Small molecule inhibition of DDAH1 significantly attenuates triple negative breast cancer cell vasculogenic mimicry *in vitro*

Julie-Ann Hulin[a,b,*], Sara Tommasi[a], David Elliot[a], Arduino A. Mangoni[a]

[a] Clinical Pharmacology, College of Medicine and Public Health, Flinders University and Flinders Medical Centre, Bedford Park, South Australia, Australia
[b] Flinders Centre for Innovation in Cancer, Bedford Park, South Australia, Australia

ARTICLE INFO

Keywords:
DDAH1
Nitric oxide
Vasculogenic mimicry
Breast cancer
ADMA

ABSTRACT

Dimethylarginine dimethylaminohydrolase 1 (DDAH1) is a key enzyme involved in the metabolism of the endogenous nitric oxide synthase (NOS) inhibitors asymmetric dimethylarginine (ADMA) and monomethyl arginine (L-NMMA). Increased DDAH1 expression and subsequent increased NO production have been recently linked to cancer. Specifically, DDAH1 is implicated in establishment of a vascular network by tumour cells, vasculogenic mimicry (VM), which is strongly associated with tumour progression and poor patient prognosis. The use of DDAH1 inhibitors as potential therapeutic agents thus represents a growing field of interest. Here we describe a UPLC-MS assay to quantify stability and intracellular concentration of two small molecule DDAH1 inhibitors synthesised by our group, ZST316 and ZST152, following incubation with MDA-MB-231 breast cancer cells. In an *in vitro* assay of VM, both DDAH1 inhibitors significantly attenuated formation of capillary-like tube structures in a dose-dependent fashion. This was not due to cell toxicity or altered cell proliferation, but may be due in part to inhibition of cell migration. Mechanistically, we demonstrate significant modulation of the endogenous DDAH/ADMA/NO pathway following exposure of 100 μM ZST316 or ZST152: a 40% increase in the DDAH1 substrate ADMA, and a 38% decrease in the DDAH1 product L-citrulline. This study represents the first evidence for therapeutic inhibition of DDAH1 by small molecules in breast cancer.

1. Introduction

Breast cancer is the most commonly diagnosed cancer among women and at recent estimates accounted for 14.7% of cancer-related deaths worldwide [1]. A subset of breast cancers are negative for estrogen receptor (ER), progesterone receptor (PR) and human epidermal growth factor receptor 2 (HER2). This particular subtype, called triple negative breast cancer (TNBC), presents as a highly proliferative and aggressive disease for which there is currently no targeted therapy [2,3]. When compared to other molecular subtypes, TNBC results in significantly higher metastases and mortality rates and a reduced life expectancy.

Local tumour growth and distant metastasis of a solid tumour is dependent upon a specific vascular supply [4]. The sprouting and extension of pre-existing blood vessels into a tumour, angiogenesis, represents the most well-accepted paradigm for development of intratumoural vascular networks [5,6]. Whilst anti-angiogenic treatments for solid tumours have received much attention, studies have revealed that the benefits obtained are variable among cancer types, are often modest and are not beneficial in regards to long-term survival [7,8]. In particular, anti-angiogenic treatments for metastatic breast cancer have consistently failed to significantly impact overall patient survival [9–11]. Vasculogenic mimicry (VM) describes an alternative mechanism by which highly aggressive tumours can acquire a microcirculation: the formation of vessel-like networks lined by the tumour cells, effectively mimicking a true vascular endothelium [12–14]. This process occurs *de novo*, without the need for endothelial cells and independent of traditional angiogenesis [15]. Additionally, the tumour-lined vessels are able to fuse to the conventional vascular network to provide adequate blood supply for tumour growth [16]. VM networks have been demonstrated to be predictive of poor survival and increased metastatic potential through entrance of tumour cells into the vasculature [17,18]. Moreover, inhibition of VM abrogates tumour development [19].

Nitric oxide (NO) is an important cellular signalling molecule with various roles in many physiological processes such as angiogenesis [20], but also with roles related to the onset and progression of pathological states including septic shock [21], pulmonary fibrosis [22]

* Corresponding author at: Clinical Pharmacology, College of Medicine and Public Health, Flinders University and Flinders Medical Centre, Bedford Park, South Australia, Australia.
E-mail address: julieann.hulin@flinders.edu.au (J.-A. Hulin).

https://doi.org/10.1016/j.biopha.2018.12.117
Received 5 October 2018; Received in revised form 14 December 2018; Accepted 29 December 2018

and cancer [23]. The role of NO in angiogenesis is clear: an inhibition of apoptosis [24], and an enhancement of endothelial cell proliferation and migration [25,26]. In cancer, NO has diverse roles and the effects are proposed to be dual (pro- and anti-tumour) depending on local concentration [27]. In many cancers, including those of the breast, NO has been positively correlated with tumour grade and a pathological role for NO in maintaining tumour blood supply has been identified [28,29]. Synthesis of NO is tightly regulated by the family of nitric oxide synthase (NOS) enzymes through conversion of arginine to NO and L-citrulline. In turn, the activity of all NOS isoforms is decreased by the methylated arginines asymmetric dimethylarginine (ADMA) and monomethyl arginine (L-NMMA), which act as competitive endogenous inhibitors [30,31]. Dimethylarginine dimethylaminohydrolase (DDAH), expressed in mammalian cells as one of two isoforms, DDAH1 or DDAH2, accounts for > 80% of the *in vivo* metabolism of ADMA and L-NMMA; current evidence suggests that DDAH1 is the primary isoform for ADMA and L-NMMA clearance [32–34]. Overexpression of DDAH1 thus results in a decrease in ADMA concentrations and subsequent increase in NO production. This has been shown to enhance vascularisation of tumours, which is accompanied by an increase in tumour growth and metastatic potential [35–37]. Current literature reports identify DDAH1 as a potential therapeutic target; we and others have demonstrated a significant increase in DDAH1 expression in melanoma [38], prostate [39] and breast [40] cancers. Additionally, we have recently shown that siRNA-mediated knockdown of DDAH1 expression in the TNBC MDA-MB-231 cell line not only increases endogenous cellular ADMA concentrations but also decreases tube formation in an *in vitro* assay of VM by up to 80% [40]. These studies raise the question as to whether the pharmacological inhibition of DDAH1 activity could be used to limit NO production and reduce VM potential.

To date, pharmacological inhibition of DDAH1 in breast cancer has not been studied. Here, we have utilised two potent DDAH1 small molecule inhibitors synthesised within our lab and described previously: arginine analogues ZST316 and ZST152 [41,42]. The aims of this study were to develop a sensitive and reproducible UPLC-MS assay to quantify ZST316 and ZST152 stability and cellular uptake in breast cancer cells, and to assess the subsequent biological response with regard to VM and cellular changes in components of the DDAH/ADMA/NO pathway. Our data suggests that inhibition of DDAH1 by ZST316 and ZST152 may have therapeutic potential in solid tumours such as breast cancer which are characterised by excessive NO production.

2. Materials and methods

2.1. DDAH1 inhibitors and reagents

L-NMMA (CAS 53308-83-1; 53308-83-1, Cayman Chemical), SDMA (CAS 10278324-4; 330-24253, Enzo Life Sciences), L-Citrulline-d7 (CAS 372-75-8; C535703, Toronto Research Chemicals) and ADMA-d6 (CAS 1313730-20-9; D463577, Toronto Research Chemicals) were purchased from Sapphire Bioscience. The DDAH1 inhibitors used in this study were compounds ZST316 (2-amino-5-(3-(2-methoxyethyl)guanidino)-N-(methylsulfonyl)-pentanamide) and ZST152 (5-oxo-1,2,4-oxadiazole 1-[4-amino-4-(5-oxo-4,5-dihydro-1,2,4-oxadiazol-3-yl)butyl]-3-(2-methoxyethyl)guanidine) (Fig. 1). Both the synthesis and the pharmacological evaluation of these inhibitors towards DDAH1 in an isolated system have been previously published [41,42].

2.2. Breast cancer cell lines

The human breast cancer cell line MDA-MB-231 was purchased from the American Type Culture Collection (ATCC; www.atcc.org) and maintained in Dulbecco's Modified Eagle Medium (DMEM) supplemented with 10% foetal bovine serum (FBS). The human breast cancer cell line BT549 was provided by the laboratory of Dr. Marina Kochetkova at the University of Adelaide, South Australia, and maintained in RPMI 1640 medium supplemented with 10% FBS. Both cell lines were maintained at 37 °C and 5% CO_2.

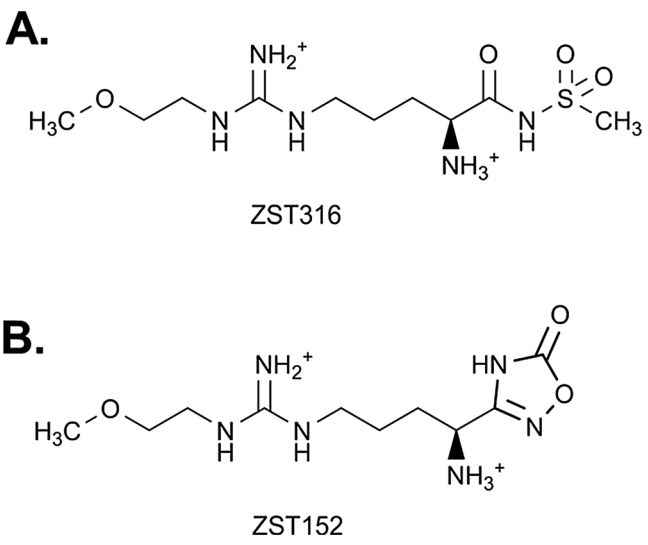

Fig. 1. Chemical structures of the DDAH1 inhibitors (A): ZST316 and (B): ZST152.

2.3. Matrigel tube formation assays

Cells were plated at $3*10^5$ cells/well in 6-well plates and allowed to adhere for 24 h. Following attachment, cells were pre-treated with DDAH1 inhibitors, L-NMMA (positive control) or SDMA (negative control) for a further 24 h. Matrigel® (Corning) aliquots were thawed overnight on ice and 45 µL per well used to coat wells of a 96-well plate. The Matrigel layer was allowed to gel by incubating the plate at 37 °C for 30 min. Twenty-four hours post incubation with the compounds, cells were resuspended and seeded in serum-free media at $2.5*10^4$ cells/well in a total volume of 150 µL in Matrigel-coated wells. The effect of the pharmacological agents on tube formation was assessed after 20 h. Wells were imaged with an EVOS® FL imaging system (Life Technologies) using a 2x objective. Four or five images per well were stitched together and the total number of tubes and branches counted using ImageJ software (NIH). Tube-like structures were defined as elongated multi-cellular structures and branches defined as the intersecting points of two or more tubes.

2.4. Cell viability and proliferation

For assessment of cell viability and proliferation by the IncuCyte™ monitoring system (Essen Bioscience), cells were seeded in complete media (10% FBS) at $1.6*10^4$ cells/well in 48-well plates. Twenty-four hours post-seeding, DDAH1 inhibitors were added to wells at concentrations of 0, 0.1, 1, 10, 100 and 250 µM in either complete media or in serum-free conditions. Cell confluence was measured across 4 images per well, every 2 h for a 48 h period from addition of inhibitors.

2.5. Scratch wound migration assays

Cells were seeded at $2*10^5$ cells/well in 24-well plates. Twenty-four hours post-seeding, DDAH1 inhibitors were added to wells at 100 µM final concentration. The following day, confluent cells were serum starved for 4 h prior to wound generation. Wounds were created using a WoundMaker™ (Essen Bioscience) and cells were washed twice to remove debris. Vehicle or inhibitors (100 µM) were added to cells in DMEM supplemented with 0.5% FBS. Wells were imaged with an EVOS® FL imaging system (Life Technologies) using a 2x objective at 0, 5, 10 and 24 h time points. Wound area at each time point was

Table 1
Internal standard concentrations and dilutions applied in stability experiments.

Compound tested	Concentration tested (μM)	Internal standard	Concentration of internal standard solution (μM)	Dilution
ZST316	0.1	ZST152	0.25	Undiluted
	1		2.5	1:10
	10		25	1:100
ZST152	0.1	ZST316	0.25	Undiluted
	1		2.5	1:10
	10		25	1:100

quantified using the automated 'find edges' function within ImageJ software (NIH) to detect the position of the leading edge; the area enclosed by the detected leading edge was calculated by the measurement function.

2.6. DDAH1 inhibitor stability and uptake

For assessment of DDAH1 inhibitor (ZST316 and ZST152) stability, compounds were added to 2 mL DMEM (+/- serum) in a 6-well plate at concentrations of 0.1, 1 and 10 μM and incubated for 24 h at 37 °C, 5% CO_2. At selected incubation times (0, 2, 6 and 24 h), a 40 μL aliquot was removed from each well and added to 10 μL of an ice-cold solution of internal standard (IS) (see Table 1). Protein precipitation was achieved via the addition of 200 μL 0.1% formic acid in isopropanol followed by 1 min vortex mixing, cooling in an ice bath for 5 min and centrifuging for 3 min at 18,000 x g. Prior to analysis the supernatant of the higher concentration samples were diluted in a solution of 1:5 water/0.1% formic acid in isopropanol (see Table 1 for dilution ratios). Calibrators were prepared by either spiking ZST316 (0–100 nM) into a comparable biological matrix and using ZST152 (250 nM) as the IS, or by spiking ZST152 (0–100 nM) and using ZST316 (250 nM) as the IS. Calibrators were treated as above without the dilution step. A 5 μL aliquot was used for UPLC-MS analysis. Calibration curves for ZST316 and ZST152 were constructed by plotting the peak area ratio analyte to IS versus the IS concentration. Precision of the method was determined by spiking 30 and 80 nM ZST316 or ZST152 into complete culture medium.

For intracellular analysis of ZST316 and ZST152, MDA-MB-231 cells were cultured under conditions closely mimicking those of the matrigel tube formation assays. Cells were seeded at $4*10^5$ in T25 flasks and incubated with vehicle or 100 μM DDAH1 inhibitors for 24 h in complete media, followed by fresh compound for 24 h in serum-free media for a total of 48 h. Cultured cells were thoroughly washed and lysed in 270 μl ice-cold water containing 2 μM L-citrulline-d7 and 0.5 μM ADMA-d6 as IS. Cell lysis was achieved by sonication with 6 × 5 s bursts at 40% amplitude (Sonics Vibracell) followed by addition of 810 μL 0.1% formic acid in methanol. Calibrators were prepared by spiking citrulline (0–375 nM), ADMA (0–75 nM), ZST316 (0–1.5 μM) and ZST152 (0–1.5 μM) into a comparable biological matrix; untreated MDA-MB-231 cells grown and lysed under the same conditions were used to prepare matrix-matched calibrators. Samples and calibrators were vortex mixed for 3 min, held on ice for 30 min and vortexed for a further 3 min. Protein and cellular debris was pelleted by centrifugation at 18,000 x g for 5 min and supernatant was transferred to 12 × 75 mm borosilicate glass tubes. Solvent was removed by evaporation in a MiVac concentrator (T = 46 °C, P = 30 mbar, −OH programme, 90 min). The residue was redissolved in 180 μL of a 1:4 water/0.1% formic acid in methanol mixture and 5 μL injected for UPLC-MS analysis.

2.7. UPLC-MS analysis

Analysis of concentrations of ZST316, ZST152, citrulline, ADMA, arginine and ornithine was performed on a Waters ACQUITY™ Ultra Performance LC™ system coupled to a Waters Premier quadrapole time of flight (qToF) mass spectrometer with an electrospray ionisation source operated in positive ionisation mode. Time of flight (ToF) data were collected between 50 and 1000 Da with an instrument scan time of 0.8 s. Experimental parameters were as follows: capillary voltage 3.0 kV, source temperature 100 °C, desolvation temperature 300 °C, sampling cone voltage 24.0 eV, extraction cone voltage 5.0 eV, cone gas flow 30 L/hr, desolvation gas flow 400 L/hr, collision cell entrance 2.0, collision exit -10, collision gas flow 0.6 ml/min. Parent and selected fragment ions were used for detection and quantitation of each analyte. Instrument control, data acquisition and data processing were performed using Waters MassLynx version 4.1 software. Chromatographic separation was performed at a flow rate of 0.4 ml/min on a Waters Atlantis HILIC column (3 μm, 2.1 mm x 150 mm). Mobile phase composition was 0.1% formic acid in acetonitrile (mobile phase A) and 10% acetonitrile, 0.1% formic acid and 10 mM ammonium formate in water (mobile phase B). Initial conditions were 95% mobile phase A and 5% mobile phase B. The proportion of mobile phase B was increased linearly to 50% over 16 min and then returned to 5% for 4 min to re-establish equilibrium before injection of the following sample.

Extracted ion chromatograms (EICs) were obtained with a mass window of 0.02 Da from total ion chromatograms (TIC) using *m/z* of 310.24 (ZST316), 273.24 (ZST152), 133.14 (ornithine), 175.16 (arginine), 203.21 (ADMA) and 209.25 (ADMA-d6); all corresponding to the parent ions. For citrulline analysis, ion chromatograms were extracted at *m/z* 159.12 and 166.16 corresponding to the 176.10→159.12 and 181.13→166.16 fragments of L-citrulline and L-citrulline-d7, respectively. Citrulline-d7 was used as the IS for the quantification of all analytes except ADMA (See Table 2).

2.8. Statistical analysis

Data are shown as mean ± SEM. Statistical analysis between groups was performed using an independent two-tailed Student's *t* test, one-way ANOVA or two-way ANOVA as appropriate. All analyses were performed using GraphPad Prism 6 (GraphPad Software). A *p* value of less than 0.05 was considered to be statistically significant.

3. Results

3.1. Stability and intracellular detection of the DDAH1 inhibitors ZST316 and ZST152

The stability of compounds ZST316 and ZST152 in cell culture

Table 2
Summary of UPLC-MS quantitative parameters.

Analyte	RT (min)	Ion	m/z (Da) [a,b]	Int Std	LOD (nM)	LOQ (nM)
ADMA	12.33	parent	203.21	ADMA-d6	2	5
ADMA-d6	12.38	parent	209.25	n/a	n/a	n/a
arginine	11.49	parent	175.16	L-citrulline-d7	n/a[c]	n/a[c]
L-citrulline	9.68	fragment	159.12	L-citrulline-d7	3	10
L-citrulline-d7	9.74	fragment	166.16	n/a	n/a	n/a
ornithine	11.87	parent	133.14	L-citrulline-d7	n/a[c]	n/a[c]
ZST152	9.34	parent	273.24	L-citrulline-d7	3	10
ZST316	9.05	parent	310.24	L-citrulline-d7	4	12

Legend: ADMA, asymmetric dimethylarginine; LOD, limit of detection; LOQ, limit of quantitation; n/a, not applicable.

[a] *m/z* is for the positively charged analyte ion, that is $[M+H]^+$.

[b] MS data was obtained with CE = 3 V and extracted with a mass window of 0.02 Da.

[c] For arginine and ornithine, relative concentration was used for comparison between samples based on peak area ratio arginine:L-citrulline-d7 and ornithine:L-citrulline-d7, respectively. Signal to noise ratio was greater than 1000:1 for arginine and was greater than 10:1 for ornithine.

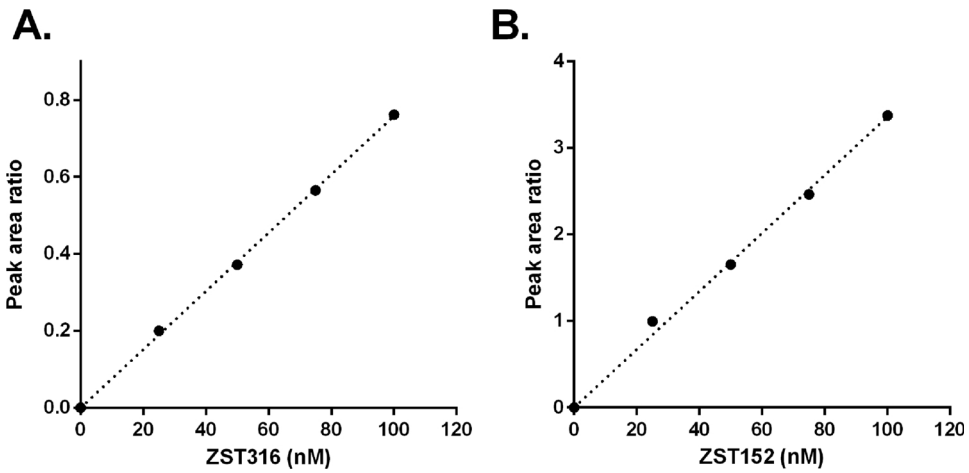

Fig. 2. Development of ZST316 and ZST152 UPLC-MS detection assay. ZST316 and ZST152 concentrations for matrix-matched (DMEM + 10% FBS) calibrators were between 0 and 100 nM. **(A):** Representative ZST316 calibration curve. **(B):** Representative ZST152 calibration curve.

media at 37 °C and their subsequent recovery has not previously been examined. In order to assess this, we first developed a method for analysis of ZST316 and ZST152 concentration. Quantification was linear between 0 and 100 nM for both ZST316 and ZST152 (Fig. 2), with a limit of detection (LOD) of approximately 4 nM and a limit of quantitation (LOQ) of approximately 12 nM for both compounds. The LOD was calculated as the analyte concentration corresponding to 3:1 signal to noise ratio, whilst the LOQ was calculated as the analyte concentration corresponding to 10:1 signal to noise ratio. The whole assay %CV was less than 11% for both ZST316 and ZST152 at both 30 and 80 nM.

To assess ZST316 and ZST152 stability, the compounds were added at concentrations of 0.1, 1, and 10 μM to individual wells containing DMEM (+/- serum). Plates were cultured for up to 24 h at 37 °C and 5% CO_2, and ZST316 and ZST152 concentration was determined. At all concentrations and timepoints assessed we observed no significant change in recovery, and no degradation, of both ZST316 and ZST152 from the culture media (Table 3). We then assessed the cellular uptake of ZST316 and ZST152 with the breast cancer cell line, MDA-MB-231. Following 48 h of incubation with 100 μM ZST316 or ZST152, cells were washed to remove extracellular compound, then lysed to release the intracellular compounds. The intracellular concentration of ZST316 and ZST152 was determined using the established UPLC-MS assay. Retention times for the DDAH1 inhibitors were 9.05 min for ZST316 and 9.34 min for ZST152 (Fig. 3A and B) and calibration curves were linear between 0 and 1.5 μM (Fig. 3C and D). The concentrations of ZST316 and ZST152 in the assay cell lysates were 0.32 μM and 0.28 μM respectively. These concentrations translated to an average ZST316 intracellular concentration of 39 pmol/million cells (Fig. 3E) and an average ZST152 intracellular concentration of 35 pmol/million cells (Fig. 3F).

3.2. ZST316 and ZST152 inhibit tube formation by breast cancer cells

Our previous work identified a key role for DDAH1 in the promotion of VM in breast cancer cell lines [40]. We therefore sought to identify what impact intracellular ZST316 and ZST152 may have on the cells in regards to this process. Consistent with our previous observations, vehicle-treated MDA-MB-231 cells formed an extensive network of tube-like structures within 20 h of seeding on Matrigel, thus mimicking the behaviour of endothelial cells and demonstrating a high capacity to undertake VM (Fig. 4; vehicle controls). To assess the effect of ZST316 and ZST152 on tube formation, cells were pre-incubated with increasing concentrations of the compounds (0.1, 1, 10, 100 and 250 μM) for 24 h prior to seeding on Matrigel. The compounds were then added again to fresh media upon seeding and tube formation was assessed 20 h later. Compared to vehicle-treated cells, we observed no change in the number of tubes or branches formed by cells incubated with 0.1 μM ZST316. A significant reduction in the number of tubes (18.5%) and branches (15%) was observed when cells were incubated with 1 μM ZST316, and a further reduction (15% and 17% respectively) was apparent when cells were incubated with 100 μM ZST316. No further inhibition of tube formation was observed at 250 μM (Fig. 4A and B). Importantly, we were able to determine that this was not a cell-specific

Table 3
Recovery of ZST316 and ZST152 from tissue culture media.

Media	Compound	Concentration (μM)	Recovery (%) ± SD			
			0 hr	2 hr	6 hr	24 hr
10% FBS	ZST316	0.1	100 ± 3.8	96.95 ± 2.4	97.13 ± 1.66	114.16 ± 2.68
		1	100 ± 9.72	97.29 ± 0.59	97.85 ± 2.31	103.61 ± 4.88
		10	100 ± 7.11	96.21 ± 2.74	97.66 ± 8.93	98.24 ± 7.23
	ZST152	0.1	100 ± 1.30	107.90 ± 12.08	101.73 ± 9.33	93.34 ± 3.65
		1	100 ± 1.75	107.92 ± 16.92	100.57 ± 1.57	104.05 ± 8.49
		10	100 ± 11.77	99.77 ± 8.13	90.78 ± 1.44	90.32 ± 8.65
Serum free	ZST316	0.1	nd	nd	nd	nd
		1	100 ± 10.92	97.44 ± 7.79	94.8 ± 8.79	102.68 ± 1.02
		10	100 ± 1.04	99.12 ± 1.14	86.73 ± 8.22	97.51 ± 6.97
	ZST152	0.1	100 ± 8.37	99.48 ± 0	107.58 ± 2.29	93.91 ± 11
		1	100 ± 0.82	93.49 ± 9.35	104.41 ± 4.55	103.27 ± 6.1
		10	100 ± 14.48	93.85 ± 3.94	100.3 ± 4.29	109.35 ± 0

nd: no data.

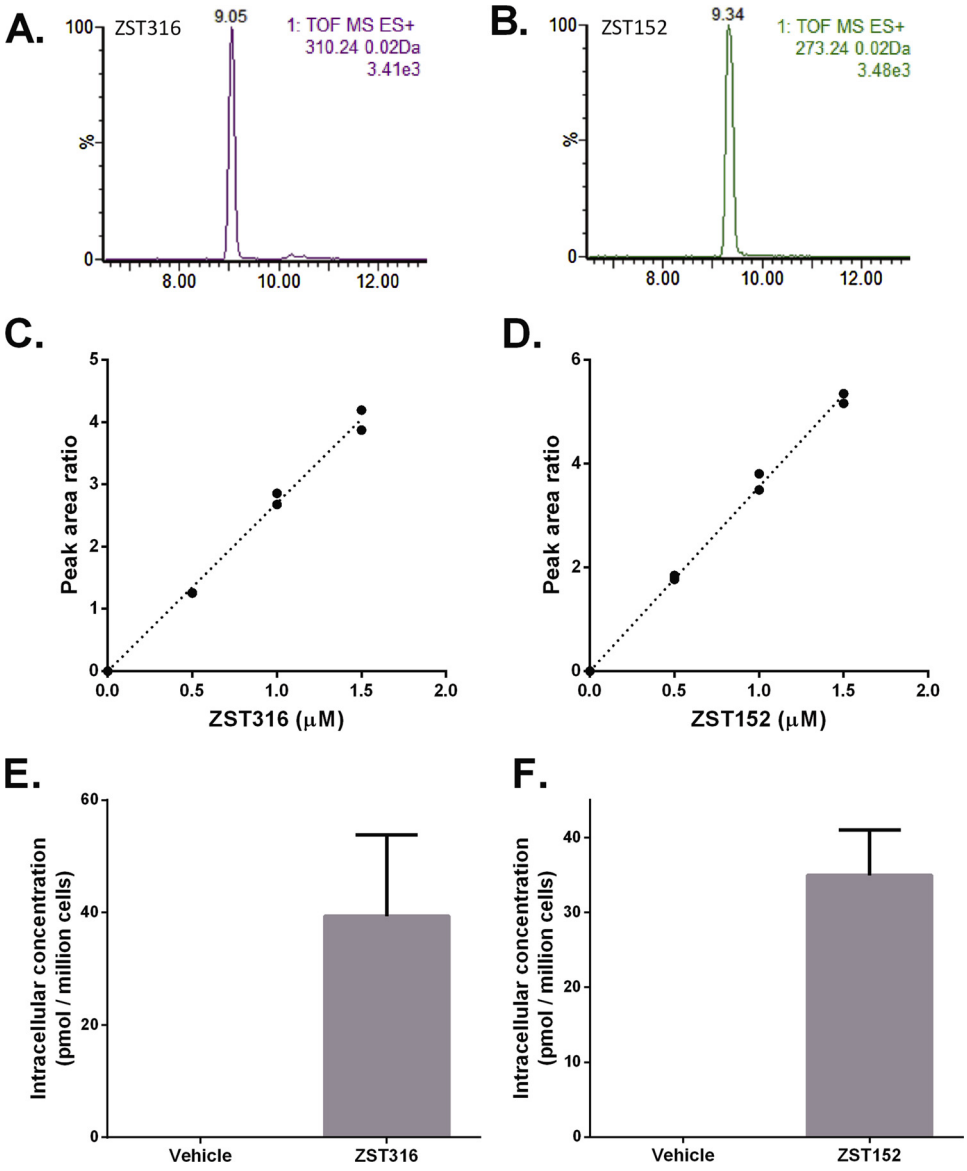

Fig. 3. Intracellular detection of ZST316 and ZST152 in MDA-MB-231 cells. **(A):** Representative chromatogram for ZST316 extracted at 310.24 Da. **(B):** Representative chromatogram for ZST152 extracted at 273.24 Da. **(C,D):** Representative calibration curves for ZST316 (C) and ZST152 (D). ZST316 and ZST152 concentrations for matrix-matched calibrators were between 0 and 1.5 μM and samples were run in duplicate. **(E):** Intracellular concentration of ZST316 following treatment of MDA-MB-231 cells with 100 μM ZST316 for 48 h. **(F):** Intracellular concentration of ZST152 following treatment of MDA-MB-231 cells with 100 μM ZST152 for 48 h. Concentrations are expressed as pmol/million cells. Data shown are mean of triplicate samples. Error bars represent SD.

result; 100 μM ZST316 also significantly reduced tube and branch formation by approximately 30% in another breast cancer cell line, BT549 (Fig. 5). MDA-MB-231 cells incubated with ZST152 displayed a similar trend as those incubated with ZST316 in terms of VM potential. Cells which were treated with 0.1 μM ZST152 formed the same number of tubes and branches as vehicle-treated cells. Cells incubated with 1 μM ZST152 formed significantly less tubes (21%) and branches (20%), however increasing concentrations of ZST152 had no further significant reduction on tube formation (Fig. 4C and D).

In addition to ZST316 and ZST152, we also assessed the effect of increased cellular L-NMMA and SDMA on tube formation of MDA-MB-231 cells. In both cases we chose concentrations that are considered physiologically relevant, pathologically relevant, and an additional considerably higher concentration; 0.05, 10 and 1000 μM for L-NMMA and 0.5, 1 and 10 μM for SDMA [43]. Treatment of cells with L-NMMA resulted in a significant inhibition of tube and branch formation at the lowest concentration tested (0.05 μM; 11%) up to 38% inhibition at 1000 μM (Fig. 4E and F). As expected, SDMA, which is neither a substrate for DDAH1 nor an inhibitor of NOS activity [44] did not significantly inhibit tube formation of MDA-MB-231 cells at any concentration tested (Fig. 4G and H). In all cases where an inhibition of tube formation was observed, cells were more likely to remain as single or tightly clustered cells and to form longer, less networked tubes.

3.3. ZST316 and ZST152 inhibit cell migration but not proliferation

In order to rule out the possibility of a change in *in vitro* vasculogenic activity being due to altered cell survival or proliferation, we assessed toxicity of the DDAH1 inhibitors ZST316 and ZST152 toward MDA-MB-231 cells under both serum and serum-free conditions. Using the Incucyte™ imaging system, cells were treated with vehicle, 0.1, 1, 10 or 100 μM of either ZST316 or ZST152 and imaged every 4 h over a 48 h period. There was no change in cell viability or proliferation with any concentration used in this study (Fig. 6) (Data not shown for 0.1–10 μM). As expected, minimal cell proliferation was observed in serum-free conditions. We also assessed the effect of DDAH1 inhibition by ZST316 and ZST152 on cell migration by means of a scratch wound assay. Quantification of wound size at 0, 5, 10 and 24 h timepoints revealed a statistically significant delay in wound closure time for cells treated with 100 μM ZST316 or ZST152 relative to vehicle (Fig. 6E and F).

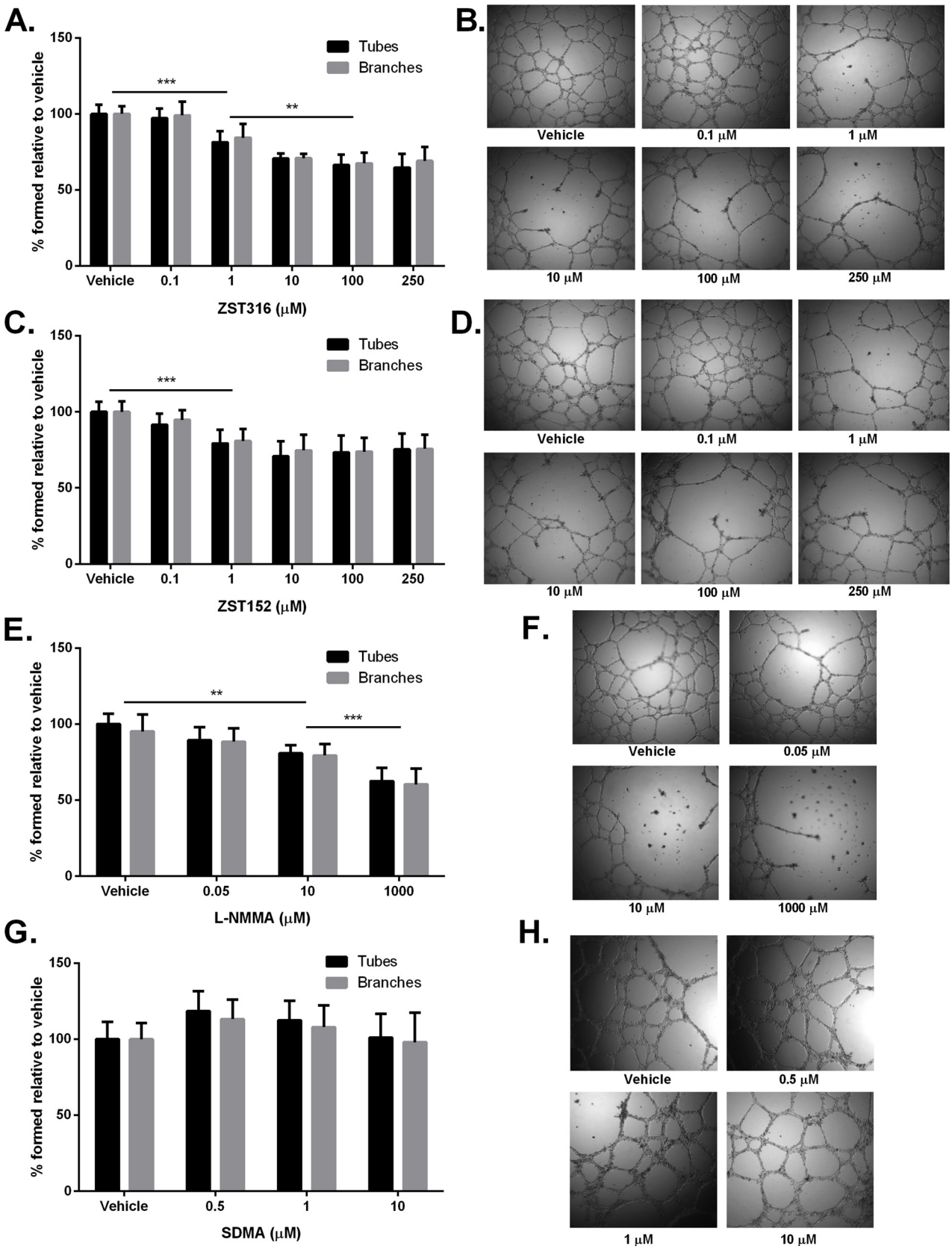

Fig. 4. ZST316 and ZST152 attenuate formation of tube-like structures by MDA-MB-231 cells on Matrigel. MDA-MB-231 cells were pre-incubated with vehicle, DDAH1 inhibitors, L-NMMA or SDMA for 24 h, seeded on Matrigel and treated for a further 24 h. The number of tubes and branches were counted following incubation with ZST316 **(A, B)**, ZST152 **(C, D)**, L-NMMA **(E, F)** and SDMA **(G, H)** and are expressed as a % relative to vehicle control. Representative phase contrast images are shown. Data shown are mean of two independent experiments performed in quadruplicate. Error bars represent SD. ** $p < 0.01$, *** $p < 0.001$.

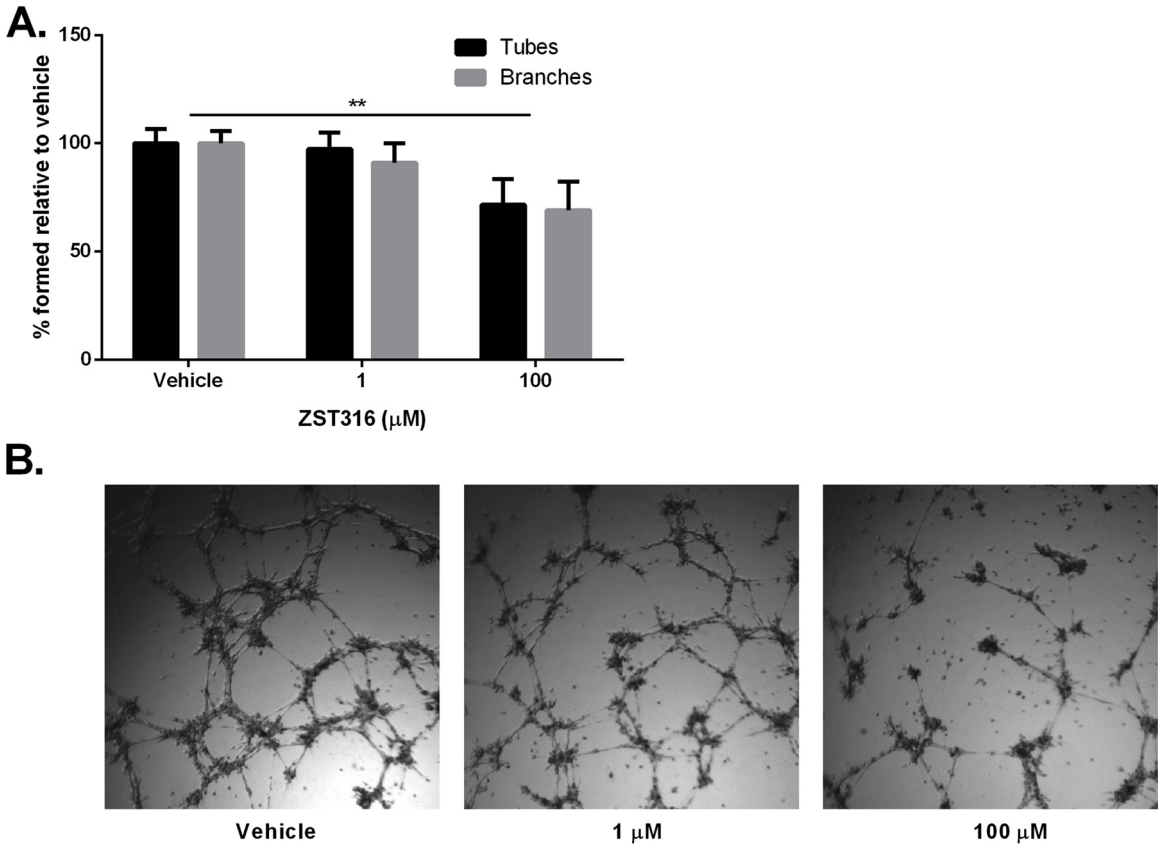

Fig. 5. ZST316 attenuates formation of tube-like structures by BT549 cells on Matrigel. (A): BT549 cells were pre-incubated with vehicle or ZST316 for 24 h, seeded on Matrigel and treated for a further 24 h. The number of tubes and branches were counted following incubation and are expressed as a % relative to vehicle control. Data shown are mean of one independent experiment performed in quadruplicate. Error bars represent SD. ** $p < 0.01$. (B): Representative phase contrast images.

3.4. Evidence of DDAH1 inhibition by ZST316 and ZST152

After demonstrating detection of ZST316 and ZST152 intracellularly, coupled with an observed biological effect in VM tube formation assays, we sought to identify whether these data could be corroborated by a UPLC-MS based assay used to quantify components of the DDAH/NOS pathway. Treatment of MDA-MB-231 cells with 100 μM ZST316 or ZST152 for 48 h caused a significant elevation of the DDAH1 endogenous substrate, ADMA, increasing the intracellular concentration by approximately 40% (Fig. 7A) compared to cells that received vehicle. Furthermore, cells incubated with the small molecules had an approximate 36–38% reduction in L-citrulline concentration (Fig. 7B). We observed no change in arginine or ornithine concentrations following incubation with either ZST316 or ZST152 (Fig. 7C and D). Retention times for ADMA and L-citrulline were 12.33 min and 9.68 min respectively (Fig. 7E and F). Calibration curves were linear between 0 and 100 nM for ADMA and between 0 and 500 nM for citrulline (Fig. 7G and H).

4. Discussion

Triple negative breast cancer (TNBC) accounts for approximately 1 in 5 breast cancers and is characterised by a phenotype that is both aggressive and invasive. Due to the absence of the three most commonly targeted receptors, ER, PR and HER2, patients presenting with TNBC often have poor survival due to a lack of effective targeted treatments [3]. Current research is focusing on the identification of novel therapeutic targets which may allow for pharmacological intervention.

In TNBC, increased iNOS expression has repeatedly been clinically implicated with tumour recurrence, metastasis and patient survival [45–47]. Whilst a direct inhibition of NOS presents with a significant problem of disrupting the homeostatic balance of NO-mediated processes, an indirect mediation of NOS through DDAH1 inhibition is a promising alternative strategy to limit overproduction of NO. Recently, we identified significantly increased DDAH1 expression in TNBC-derived cell lines compared to normal mammary epithelial cells. In this *in vitro* model, DDAH1 was found to play a key role in VM; specific knockdown of DDAH1 expression in the TNBC MDA-MB-231 cell line was sufficient to inhibit tube formation by up to 80%, as well as increase endogenous cellular ADMA concentrations [40].

Our group has previously reported the design, synthesis and inhibitory profile of two DDAH1 inhibitors, ZST316 and ZST152 [41,42]. Both these inhibitors exhibit significant inhibitory potential towards DDAH1 in isolated cell lysates, with ZST316 being the most potent human DDAH1 inhibitor with 'substrate-like' structure reported in the literature to date (98% inhibition at 1 mM, $IC_{50} = 3$ μM and $K_i = 1$ μM). In this study, we utilised these inhibitors to pharmacologically modulate DDAH1 activity in TNBC MDA-MB-231 cells. In order to assess the suitability of using ZST316 and ZST152 in cultured breast cancer cells, we first developed a UPLC-MS assay to quantify stability and cellular uptake of the compounds. Our method was sensitive and reproducible, with linear quantification between 0 and 100 nM, LOD of 4 nM, LOQ of 12 nM and whole assay %CV less than 11% for both ZST316 and ZST152 in culture medium. Importantly, ZST316 and ZST152 were stable under standard culture conditions of 37 °C and 5% CO_2 for the 24 h time period that was assessed; we observed complete recovery from culture media with no evident breakdown products. Despite the stability of the inhibitors, MDA-MB-231 cells incubated with 100 μM ZST316 or ZST152 for 48 h revealed intracellular concentrations of only 39 pmol/million cells ZST316 and 35 pmol/million cells ZST152. This suggests that the compounds are not efficiently translocated across the

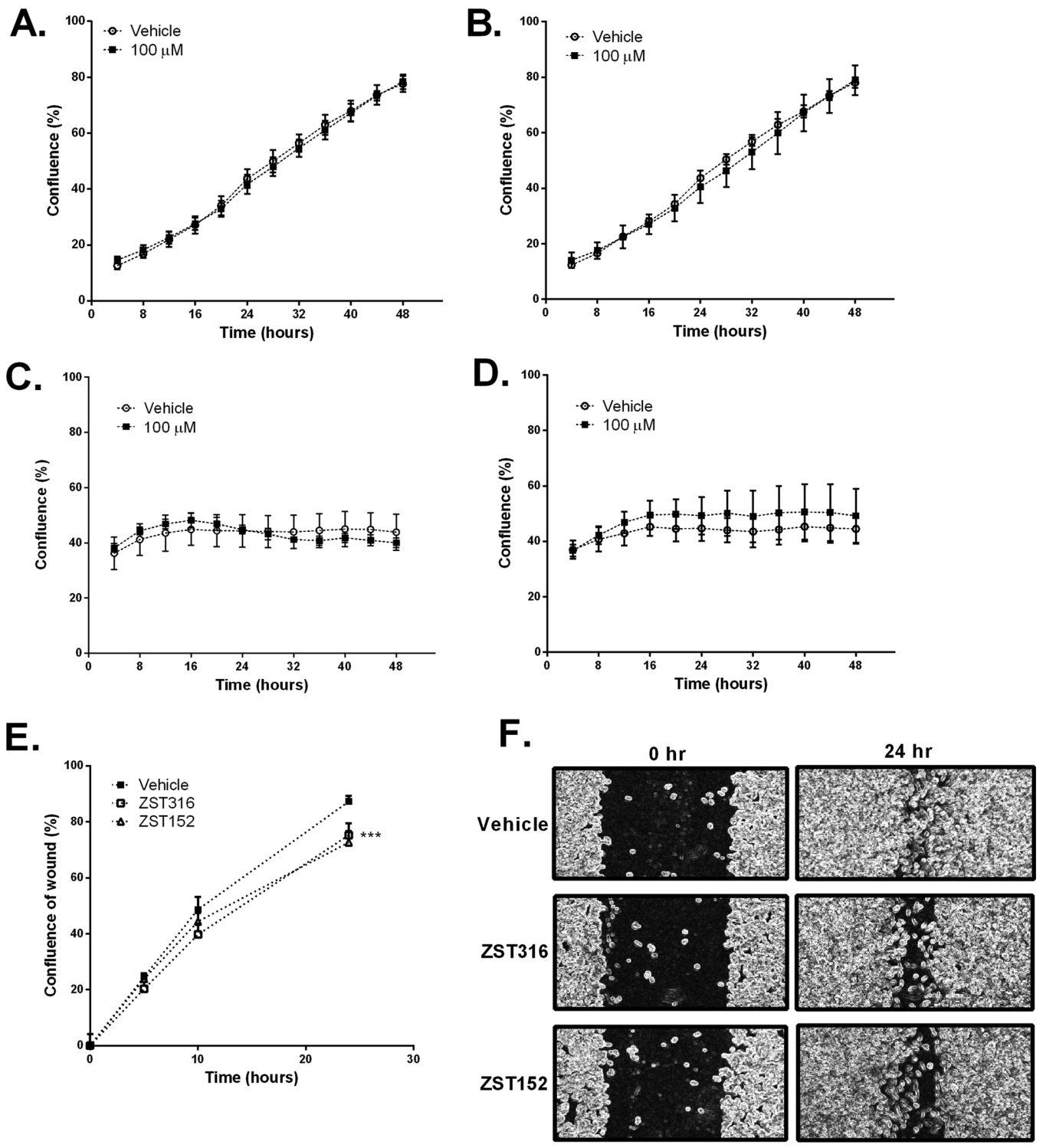

Fig. 6. ZST316 and ZST152 inhibit cell migration but not proliferation. MDA-MB-231 cells were incubated with **(A):** vehicle or 100 μM ZST316 in the presence of 10% FBS, **(B):** 100 μM ZST152 in the presence of 10% FBS, **(C):** 100 μM ZST316 in the absence of serum or **(D):** 100 μM ZST152 in the absence of serum. Proliferation was assessed using the IncuCyte™ imaging system, whereby confluence was measured every 4 h over a 48 h period. Error bars represent SD of 4 images per well from quadruplicate wells. **(E):** MDA-MB-231 cells were incubated with vehicle, 100 μM ZST316 or 100 μM ZST152 for 24 h. Scratch wound migration assays were performed over a 24 h period following generation of a wound in a confluent cell monolayer. Relative wound density was determined at 0, 5, 10 and 24 h. Error bars represent SD of 4 independent replicates. *** $p < 0.001$. **(F):** Representative images with the ImageJ 'find edges' function applied.

cell membrane and it is plausible that they are internalised by passive diffusion. Together, these data provide additional information to the pharmacokinetic profiling of ZST316 and ZST152.

Regardless of the low intracellular concentrations of ZST316 and ZST152, by employing the same UPLC-MS method, we observed a significant increase in endogenous ADMA (DDAH1 substrate, inhibitor of NOS) paired with a significant decrease in endogenous L-citrulline (DDAH1 product) following incubation with 100 μM ZST316 or ZST152. Under these conditions we did not observe any change in intracellular concentration of arginine. Mechanistically, as arginine is a

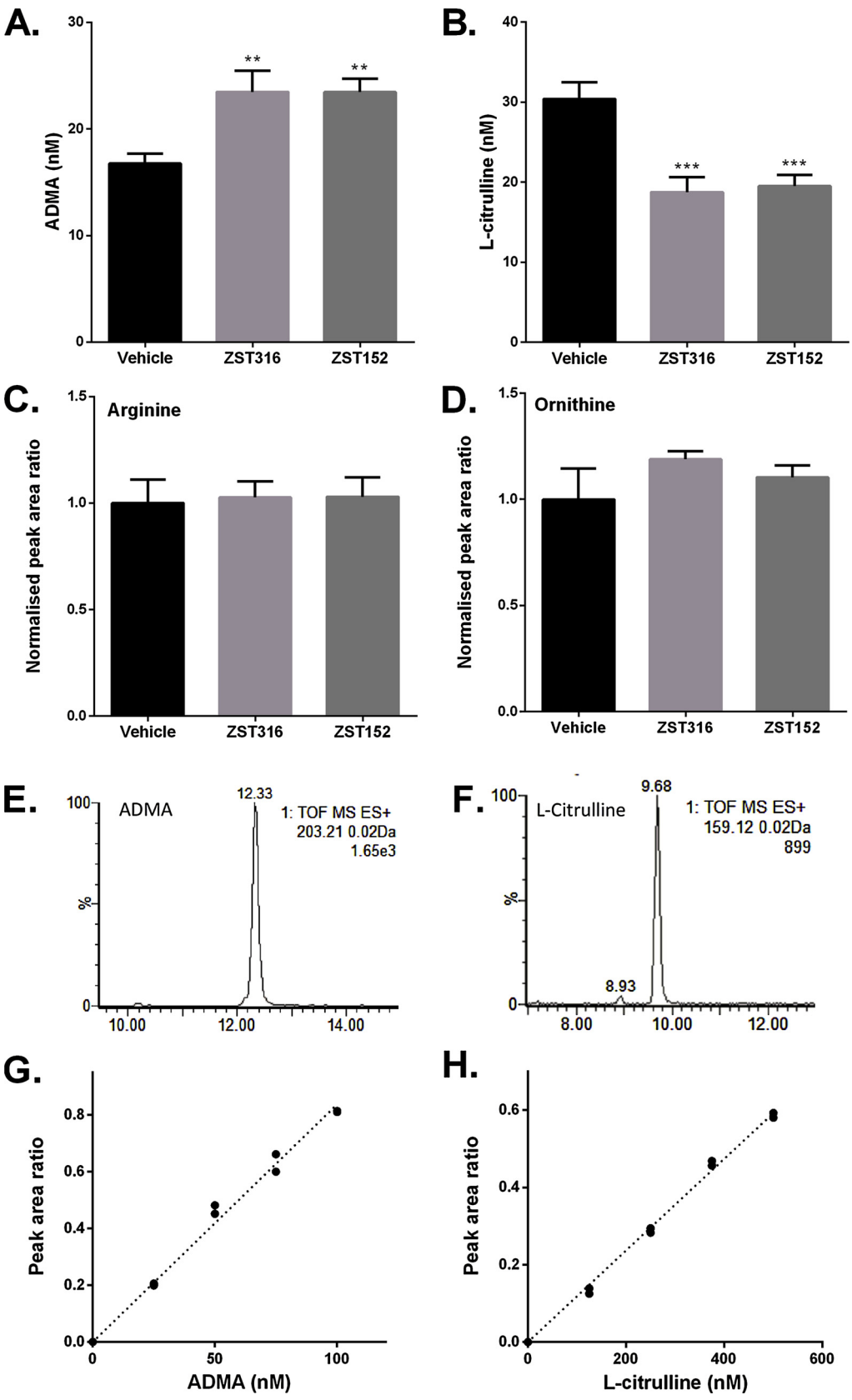

Fig. 7. Intracellular inhibition of DDAH1 activity by ZST316 and ZST152. MDA-MB-231 cells were incubated with vehicle, ZST316 or ZST152 (100 μM) for 48 h prior to cell lysis. **(A):** Intracellular ADMA concentration. **(B):** Intracellular L-citrulline concentration. **(C):** Relative intracellular arginine concentration, expressed as a fold change to the peak area ratio (arginine/d7-ADMA) of vehicle control. **(D):** Relative intracellular ornithine concentration, expressed as a fold change to the peak area ratio (ornithine/d7-ADMA) of vehicle control. Data are mean of three independent replicates. Error bars represent SEM. ** $p < 0.01$, *** $p < 0.001$ relative to vehicle controls. **(E):** Representative chromatogram for ADMA, extracted at 203.21 Da. **(F):** Representative chromatogram for L-citrulline, extracted at 159.12 Da. **(G):** Representative calibration curve for ADMA. ADMA concentration for matrix-matched calibrators was between 0 and 100 nM and samples were run in duplicate. **(H):** Representative calibration curve for L-citrulline. L-citrulline concentration for matrix-matched calibrators was between 0 and 500 nM and samples were run in duplicate.

substrate for NOS, it may be expected that indirect inhibition of NOS as a result of DDAH1 inhibition will result in increased arginine concentration. On the other hand, as arginine is also a substrate of arginase (ARG), any change in arginine concentration may be indicative of altered ARG enzymatic activity. As ZST316 and ZST152 are arginine analogues, it is important to ensure their specificity towards DDAH1, particularly in regards to off-target effects on ARG which may increase NO synthesis via increased arginine substrate availability [48]. Whilst a

comprehensive kinetic analysis of ZST316 and ZST152 inhibition towards ARG1 and ARG2 is currently underway in our laboratory, preliminary data suggests that these inhibitors do not significantly alter ARG activity [unpublished data]. Additionally, here we have further utilised our UPLC-MS assay to quantify intracellular ornithine, a product of ARG, following ZST316 and ZST152 cellular uptake. As with arginine, we also observed no significant change in ornithine concentrations.Thus, there was no change in the arginine:ornithine ratio, which has previously been suggested as a biomarker of ARG activity [49]. Taken together, our data suggest that ZST316 and ZST152 provide a direct and specific inhibition of DDAH1 with unlikely off-target effects, and that the involvement of arginine in several metabolic pathways [50] confers a steady-state concentration of arginine that may be maintained despite disrupted NOS activity. This conclusion is further supported by our previous work, whereby specific knockdown of DDAH1 with siRNA also resulted in increased endogenous ADMA and no change in intracellular arginine [40]. However, further characterisation in regards to the specificities of ZST316 and ZST152 is an area that needs additional investigation.

The ability of various aggressive cancers to produce functional blood vessels *de novo* via VM is associated with tumour progression and is a critical complement for angiogenesis. A characteristic feature of TNBC is the ability to form capillary-like tubes in a modified *in vitro* model of VM, which we have utilised in this study. Our findings that ZST316 and ZST152 have anti-VM effects in MDA-MB-231 cells is consistent with our previous report demonstrating that specific knockdown of DDAH1 protein significantly blocked VM [40]. Although the level of VM inhibition by ZST316 and ZST152 observed in this study is significantly less than that previously observed with DDAH1 knockdown, we observed a similar level of inhibition when cells were treated with the endogenous NOS inhibitor, L-NMMA. L-NMMA is widely used as a tool to decrease NO availability with an effective concentration range between 0.1–10 mM when treating cells [51]. Furthermore, it has the same, if not greater, affinity to arginine transport systems as arginine itself [52,53], suggesting that active transport of L-NMMA occurs. Importantly, SDMA, which is predominately eliminated by renal excretion [54] and is neither a substrate for DDAH1 nor an inhibitor of NOS, but can compete with arginine for cellular uptake [55,56], had no effect on VM of MDA-MB-231 cells. Combined with our UPLC-MS generated data, this lends to two ideas: the observed effect of ZST316 and ZST152 is not due to competition for arginine transport systems, and that the low concentration of the inhibitors detected intracellularly is sufficient to inhibit VM to the same degree as the actively transported endogenous NOS inhibitor L-NMMA. It is also important to note that we observed no toxicity or inhibition of cell proliferation of MDA-MB-231 cells treated with ZST316 or ZST152, which may otherwise explain the reduction of VM potential. However, we did observe a small but significant inhibition of cell migration when cells were treated with ZST316 or ZST152. This is consistent with our previous data [40], and provides further support for the role of DDAH1 in cell migration and therefore VM.

Several classes of DDAH1 inhibitors (Cl-NIO, L-VNIO, L-257 and PD404182) have been previously described in the literature and successfully used in models of melanoma and septic shock to indirectly modulate NO availability [38,57–61]. Our results presented here are in alignment with these studies. However, to our knowledge, this study is the first to address pharmacological inhibition of DDAH1 in breast cancer and to demonstrate a significant biological effect in regard to VM. In summary, this study assessed the stability and uptake of small molecule DDAH1 inhibitors ZST316 and ZST152 into TNBC MDA-MB-231 cells, along with their cytotoxicity, effect on intracellular ADMA, L-citrulline, arginine and ornithine concentrations, and their biological function in regard to VM. To the best of our knowledge, this study represents the first time pharmacological inhibition of DDAH1 has been assessed in a breast cancer model. It also complements a limited number of recent studies where sensitive and reproducible UPLC-MS methods have been utilised to quantify concentrations of intracellular DDAH/ADMA/NO pathway analytes simultaneously [62,63]. Although the molecular mechanisms that regulate VM are not entirely understood, it is likely that they overlap with classical angiogenesis and that an upregulation of angiogenesis related genes are involved [64]. With this in mind, the overexpression of DDAH1 in breast cancer is an intriguing area to pursue. There is currently a lack of effective anti-tumour VM drugs in the clinical setting, however, our data suggest that the ability to pharmacologically inhibit DDAH1 may provide a common target for simultaneous abrogation of both VM and classical angiogenesis in the breast cancer tumour microenvironment, improving therapeutic potential. In addition, it is likely that inhibition of DDAH1 would also provide benefit to treatment of other cancers characterised by excessive NO production and further study in this area is warranted.

Conflict of interest

None declared.

Author contributions

JH, ST, DE and AM participated in research design; JH, ST and DE conducted experiments and performed data analysis; JH wrote the first draft of the manuscript; JH, ST, DE and AM actively contributed to the draft revision and final version.

References

[1] J. Ferlay, I. Soerjomataram, R. Dikshit, et al., Cancer incidence and mortality worldwide: sources, methods and major patterns in GLOBOCAN 2012, Int. J. Cancer 136 (2015) E359–386, https://doi.org/10.1002/ijc.29210.
[2] K.R. Bauer, M. Brown, R.D. Cress, et al., Descriptive analysis of estrogen receptor (ER)-negative, progesterone receptor (PR)-negative, and HER2-negative invasive breast cancer, the so-called triple-negative phenotype: a population-based study from the California cancer Registry, Cancer 109 (2007) 1721–1728, https://doi.org/10.1002/cncr.22618.
[3] F. Podo, L.M. Buydens, H. Degani, et al., Triple-negative breast cancer: present challenges and new perspectives, Mol. Oncol. 4 (2010) 209–229, https://doi.org/10.1016/j.molonc.2010.04.006.
[4] J. Folkman, Tumor angiogenesis: therapeutic implications, N. Engl. J. Med. 285 (1971) 1182–1186, https://doi.org/10.1056/nejm197111182852108.
[5] W. Risau, Mechanisms of angiogenesis, Nature 386 (1997) 671–674, https://doi.org/10.1038/386671a0.
[6] D. Hanahan, J. Folkman, Patterns and emerging mechanisms of the angiogenic switch during tumorigenesis, Cell 86 (1996) 353–364.
[7] N.S. Vasudev, A.R. Reynolds, Anti-angiogenic therapy for cancer: current progress, unresolved questions and future directions, Angiogenesis 17 (2014) 471–494, https://doi.org/10.1007/s10456-014-9420-y.
[8] N. Nishida, H. Yano, T. Nishida, et al., Angiogenesis in cancer, Vasc. Health Risk Manag. 2 (2006) 213–219.
[9] J.P. Crown, V. Dieras, E. Staroslawska, et al., Phase III trial of sunitinib in combination with capecitabine versus capecitabine monotherapy for the treatment of patients with pretreated metastatic breast cancer, J. Clin. Oncol. 31 (2013) 2870–2878, https://doi.org/10.1200/jco.2012.43.3391.
[10] C.H. Barrios, M.C. Liu, S.C. Lee, et al., Phase III randomized trial of sunitinib versus capecitabine in patients with previously treated HER2-negative advanced breast cancer, Breast Cancer Res. Treat. 121 (2010) 121–131, https://doi.org/10.1007/s10549-010-0788-0.
[11] D.W. Miles, A. Chan, L.Y. Dirix, et al., Phase III study of bevacizumab plus docetaxel compared with placebo plus docetaxel for the first-line treatment of human epidermal growth factor receptor 2-negative metastatic breast cancer, J. Clin. Oncol. 28 (2010) 3239–3247, https://doi.org/10.1200/jco.2008.21.6457.
[12] R.E. Seftor, A.R. Hess, E.A. Seftor, et al., Tumor cell vasculogenic mimicry: from controversy to therapeutic promise, Am. J. Pathol. 181 (2012) 1115–1125, https://doi.org/10.1016/j.ajpath.2012.07.013.
[13] M.J. Hendrix, E.A. Seftor, A.R. Hess, et al., Vasculogenic mimicry and tumour-cell plasticity: lessons from melanoma, Nat. Rev. Cancer 3 (2003) 411–421, https://doi.org/10.1038/nrc1092.
[14] R. Folberg, M.J. Hendrix, A.J. Maniotis, Vasculogenic mimicry and tumor angiogenesis, Am. J. Pathol. 156 (2000) 361–381, https://doi.org/10.1016/s0002-9440(10)64739-6.
[15] A.J. Maniotis, R. Folberg, A. Hess, et al., Vascular channel formation by human melanoma cells in vivo and in vitro: vasculogenic mimicry, Am. J. Pathol. 155 (1999) 739–752, https://doi.org/10.1016/s0002-9440(10)65173-5.
[16] K. Shirakawa, H. Kobayashi, Y. Heike, et al., Hemodynamics in vasculogenic mimicry and angiogenesis of inflammatory breast cancer xenograft, Cancer Res. 62 (2002) 560–566.

[17] Z. Cao, M. Bao, L. Miele, et al., Tumour vasculogenic mimicry is associated with poor prognosis of human cancer patients: a systemic review and meta-analysis, Eur. J. Cancer 49 (2013) 3914–3923, https://doi.org/10.1016/j.ejca.2013.07.148.
[18] E. Wagenblast, M. Soto, S. Gutierrez-Angel, et al., A model of breast cancer heterogeneity reveals vascular mimicry as a driver of metastasis, Nature 520 (2015) 358–362, https://doi.org/10.1038/nature14403.
[19] R. Francescone, S. Scully, B. Bentley, et al., Glioblastoma-derived tumor cells induce vasculogenic mimicry through Flk-1 protein activation, J. Biol. Chem. 287 (2012) 24821–24831, https://doi.org/10.1074/jbc.M111.334540.
[20] J.P. Cooke, NO and angiogenesis, Atheroscler. Suppl. 4 (2003) 53–60.
[21] M.A. Titheradge, Nitric oxide in septic shock, Biochim. Biophys. Acta 1411 (1999) 437–455.
[22] Y.C. Hsu, L.F. Wang, Y.W. Chien, Nitric oxide in the pathogenesis of diffuse pulmonary fibrosis, Free Radic. Biol. Med. 42 (2007) 599–607, https://doi.org/10.1016/j.freeradbiomed.2006.11.031.
[23] D. Fukumura, S. Kashiwagi, R.K. Jain, The role of nitric oxide in tumour progression, Nat. Rev. Cancer 6 (2006) 521–534, https://doi.org/10.1038/nrc1910.
[24] S. Dimmeler, A.M. Zeiher, Nitric oxide-an endothelial cell survival factor, Cell Death Differ. 6 (1999) 964–968, https://doi.org/10.1038/sj.cdd.4400581.
[25] M. Ziche, A. Parenti, F. Ledda, et al., Nitric oxide promotes proliferation and plasminogen activator production by coronary venular endothelium through endogenous bFGF, Circ. Res. 80 (1997) 845–852.
[26] T. Murohara, B. Witzenbichler, I. Spyridopoulos, et al., Role of endothelial nitric oxide synthase in endothelial cell migration, Arterioscler. Thromb. Vasc. Biol. 19 (1999) 1156–1161.
[27] D.C. Jenkins, I.G. Charles, L.L. Thomsen, et al., Roles of nitric oxide in tumor growth, Proc. Natl. Acad. Sci. U. S. A. 92 (1995) 4392–4396.
[28] Sheetal Korde Choudhari, Minal Chaudhary, Sachin Bagde, et al., Nitric oxide and cancer: a review, World J. Surg. Oncol. 11 (2013) 118, https://doi.org/10.1186/1477-7819-11-118.
[29] Q.S. Ng, V. Goh, J. Milner, et al., Effect of nitric-oxide synthesis on tumour blood volume and vascular activity: a phase I study, Lancet Oncol. 8 (2007) 111–118, https://doi.org/10.1016/s1470-2045(07)70001-3.
[30] N.M. Olken, K.M. Rusche, M.K. Richards, et al., Inactivation of macrophage nitric oxide synthase activity by NG-methyl-L-arginine, Biochem. Biophys. Res. Commun. 177 (1991) 828–833.
[31] H.Q. Zhang, W. Fast, M.A. Marletta, et al., Potent and selective inhibition of neuronal nitric oxide synthase by N omega-propyl-L-arginine, J. Med. Chem. 40 (1997) 3869–3870, https://doi.org/10.1021/jm970550g.
[32] J. Leiper, M. Nandi, B. Torondel, et al., Disruption of methylarginine metabolism impairs vascular homeostasis, Nat. Med. 13 (2007) 198–203, https://doi.org/10.1038/nm1543.
[33] X. Hu, D. Atzler, X. Xu, et al., Dimethylarginine dimethylaminohydrolase-1 is the critical enzyme for degrading the cardiovascular risk factor asymmetrical dimethylarginine, Arterioscler. Thromb. Vasc. Biol. 31 (2011) 1540–1546, https://doi.org/10.1161/atvbaha.110.222638.
[34] P. Zhang, X. Hu, X. Xu, et al., Dimethylarginine dimethylaminohydrolase 1 modulates endothelial cell growth through nitric oxide and Akt, Arterioscler. Thromb. Vasc. Biol. 31 (2011) 890–897, https://doi.org/10.1161/atvbaha.110.215640.
[35] V. Kostourou, S.P. Robinson, J.E. Cartwright, et al., Dimethylarginine dimethylaminohydrolase I enhances tumour growth and angiogenesis, Br. J. Cancer 87 (2002) 673–680, https://doi.org/10.1038/sj.bjc.6600518.
[36] V. Kostourou, S.P. Robinson, G.S. Whitley, et al., Effects of overexpression of dimethylarginine dimethylaminohydrolase on tumor angiogenesis assessed by susceptibility magnetic resonance imaging, Cancer Res. 63 (2003) 4960–4966.
[37] J. Jacobi, K. Sydow, G. von Degenfeld, et al., Overexpression of dimethylarginine dimethylaminohydrolase reduces tissue asymmetric dimethylarginine levels and enhances angiogenesis, Circulation 111 (2005) 1431–1438, https://doi.org/10.1161/01.cir.0000158487.80483.09.
[38] Y. Wang, S. Hu, A.M. Gabisi Jret al., Developing an irreversible inhibitor of human DDAH-1, an enzyme upregulated in melanoma, ChemMedChem 9 (2014) 792–797, https://doi.org/10.1002/cmdc.201300557.
[39] K.G. Ronquist, G. Ronquist, A. Larsson, et al., Proteomic analysis of prostate cancer metastasis-derived prostasomes, Anticancer Res. 30 (2010) 285–290.
[40] J.A. Hulin, S. Tommasi, D. Elliot, et al., MiR-193b regulates breast cancer cell migration and vasculogenic mimicry by targeting dimethylarginine dimethylaminohydrolase 1, Sci. Rep. 7 (2017) 13996, https://doi.org/10.1038/s41598-017-14454-1.
[41] S. Tommasi, C. Zanato, B.C. Lewis, et al., Arginine analogues incorporating carboxylate bioisosteric functions are micromolar inhibitors of human recombinant DDAH-1, Org. Biomol. Chem. 13 (2015) 11315–11330, https://doi.org/10.1039/c5ob01843a.
[42] R.B. Murphy, S. Tommasi, B.C. Lewis, et al., Inhibitors of the hydrolytic enzyme dimethylarginine dimethylaminohydrolase (DDAH): discovery, synthesis and development, Molecules 21 (2016), https://doi.org/10.3390/molecules21050615.
[43] M. van Dyk, A.A. Mangoni, M. McEvoy, et al., Targeted arginine metabolomics: a rapid, simple UPLC-QToF-MS(E) based approach for assessing the involvement of arginine metabolism in human disease, Clin. Chim. Acta 447 (2015) 59–65, https://doi.org/10.1016/j.cca.2015.05.014.
[44] B. Caplin, J. Leiper, Endogenous nitric oxide synthase inhibitors in the biology of disease: markers, mediators, and regulators? Arterioscler. Thromb. Vasc. Biol. 32 (2012) 1343–1353, https://doi.org/10.1161/atvbaha.112.247726.
[45] S. Granados-Principal, Y. Liu, M.L. Guevara, et al., Inhibition of iNOS as a novel effective targeted therapy against triple-negative breast cancer, Breast Cancer Res. 17 (2015) 25, https://doi.org/10.1186/s13058-015-0527-x.
[46] P. Garrido, A. Shalaby, E.M. Walsh, et al., Impact of inducible nitric oxide synthase (iNOS) expression on triple negative breast cancer outcome and activation of EGFR and ERK signaling pathways, Oncotarget 8 (2017) 80568–80588, https://doi.org/10.18632/oncotarget.19631.
[47] E.M. Walsh, M.M. Keane, D.A. Wink, et al., Review of triple negative breast cancer and the impact of inducible nitric oxide synthase on tumor biology and patient outcomes, Crit. Rev. Oncog. 21 (2016) 333–351, https://doi.org/10.1615/CritRevOncog.2017021307.
[48] D. Schade, J. Kotthaus, B. Clement, Modulating the NO generating system from a medicinal chemistry perspective: current trends and therapeutic options in cardiovascular disease, Pharmacol. Ther. 126 (2010) 279–300, https://doi.org/10.1016/j.pharmthera.2010.02.005.
[49] Claudia R. Morris, Gregory Kato, Mirjana Poljakovic, et al., The arginine-to-ornithine ratio: biomarker of arginase activity and predictor of mortality in sickle cell disease, Blood 104 (2004) 237.
[50] S.M. Morris Jr, Arginine metabolism: boundaries of our knowledge, J. Nutr. 137 (2007) 1602s–1609s.
[51] J. Vitecek, A. Lojek, G. Valacchi, et al., Arginine-based inhibitors of nitric oxide synthase: therapeutic potential and challenges, Mediators Inflamm. 2012 (2012) 318087, , https://doi.org/10.1155/2012/318087.
[52] K.K. McDonald, R. Rouhani, M.E. Handlogten, et al., Inhibition of endothelial cell amino acid transport System y+ by arginine analogs that inhibit nitric oxide synthase, Biochim. Biophys. Acta 1324 (1997) 133–141.
[53] M.I. Forray, S. Angelo, C.A. Boyd, et al., Transport of nitric oxide synthase inhibitors through cationic amino acid carriers in human erythrocytes, Biochem. Pharmacol. 50 (1995) 1963–1968.
[54] P. Vallance, A. Leone, A. Calver, et al., Accumulation of an endogenous inhibitor of nitric oxide synthesis in chronic renal failure, Lancet 339 (1992) 572–575.
[55] E.I. Closs, F.Z. Basha, A. Habermeier, et al., Interference of L-arginine analogues with L-arginine transport mediated by the y+ carrier hCAT-2B, Nitric Oxide 1 (1997) 65–73, https://doi.org/10.1006/niox.1996.0106.
[56] M. Al Banchaabouchi, B. Marescau, I. Possemiers, et al., NG, NG-dimethylarginine and NG, NG-dimethylarginine in renal insufficiency, Pflugers Arch. 439 (2000) 524–531.
[57] M. Nandi, P. Kelly, B. Torondel, et al., Genetic and pharmacological inhibition of dimethylarginine dimethylaminohydrolase 1 is protective in endotoxic shock, Arterioscler. Thromb. Vasc. Biol. 32 (2012) 2589–2597, https://doi.org/10.1161/atvbaha.112.300232.
[58] Z. Wang, S. Lambden, V. Taylor, et al., Pharmacological inhibition of DDAH1 improves survival, haemodynamics and organ function in experimental septic shock, Biochem. J. 460 (2014) 309–316, https://doi.org/10.1042/bj20131666.
[59] J. Leiper, M. Nandi, The therapeutic potential of targeting endogenous inhibitors of nitric oxide synthesis, Nat. Rev. Drug Discov. 10 (2011) 277–291, https://doi.org/10.1038/nrd3358.
[60] J. Kotthaus, D. Schade, N. Muschick, et al., Structure-activity relationship of novel and known inhibitors of human dimethylarginine dimethylaminohydrolase-1: alkenyl-amidines as new leads, Bioorg. Med. Chem. 16 (2008) 10205–10209, https://doi.org/10.1016/j.bmc.2008.10.058.
[61] Y.T. Ghebremariam, D.A. Erlanson, J.P. Cooke, A novel and potent inhibitor of dimethylarginine dimethylaminohydrolase: a modulator of cardiovascular nitric oxide, J. Pharmacol. Exp. Ther. 348 (2014) 69–76, https://doi.org/10.1124/jpet.113.206847.
[62] S. Shin, S.K. Thapa, H.L. Fung, Cellular interactions between L-arginine and asymmetric dimethylarginine: transport and metabolism, PLoS One 12 (2017) e0178710, , https://doi.org/10.1371/journal.pone.0178710.
[63] K. Milewski, M. Bogacinska-Karas, I. Fresko, et al., Ammonia reduces intracellular asymmetric dimethylarginine in cultured astrocytes stimulating its y(+)LAT2 carrier-mediated loss, Int. J. Mol. Sci. 18 (2017), https://doi.org/10.3390/ijms18112308.
[64] K. Shirakawa, H. Tsuda, Y. Heike, et al., Absence of endothelial cells, central necrosis, and fibrosis are associated with aggressive inflammatory breast cancer, Cancer Res. 61 (2001) 445–451.